

Electronic properties of amorphous silicon carbon are correlated with the methane flow rate

Soni Prayogi¹, Yoyok Cahyono², Darminto²

¹Department of Electrical Engineering, Faculty of Industrial Technology, Pertamina University, Jakarta, Indonesia

²Department of Physics, Faculty of Natural Sciences, Institut Teknologi Sepuluh Nopember, Surabaya, Indonesia

Article Info

Article history:

Received May 26, 2024

Revised Sep 16, 2024

Accepted Oct 23, 2024

Keywords:

a-SiC:H

Flow rate

Methane

PECVD

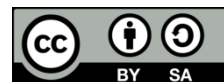
p-type

Spectroscopy ellipsometry

ABSTRACT

This study examines how methane flow rate during the plasma-enhanced chemical vapor deposition (PECVD) process affects the electronic properties of amorphous silicon-carbon (a-SiC) thin films. The films were deposited with varying methane flow rates, and their structural and electronic properties were analyzed using spectroscopic ellipsometry and atomic force microscopy (AFM). Results show that the methane flow rate influences the ratio of sp² to sp³ carbon bonding, which impacts the material's electronic band structure. Higher methane flow rates increase sp² carbon content, reducing the bandgap energy and enhancing electrical conductivity. In contrast, lower flow rates lead to higher sp³ bonding, wider band gaps, and decreased conductivity. This study highlights the potential for optimizing methane flow rates in PECVD to tailor the electronic properties of a-SiC films for specific applications. The findings offer valuable insights for designing and optimizing a-SiC materials for electronic devices. Future research will investigate how other deposition parameters and post-deposition treatments affect a-SiC's electronic properties, aiming to further improve material performance for advanced technological applications.

This is an open access article under the [CC BY-SA](#) license.



Corresponding Author:

Soni Prayogi

Department of Electrical Engineering, Faculty of Industrial Technology, Pertamina University

Tengku Nyak Arief Street, Simprug, South Jakarta, DKI Jakarta, Indonesia

Email: prayogi.sp@gmail.com

1. INTRODUCTION

The study of amorphous silicon carbon (a-SiC) has garnered significant attention due to its unique electronic properties and potential applications in various technological fields such as photovoltaic cells, light-emitting diodes (LEDs), and thin-film transistors [1]. Amorphous silicon-carbon combines the beneficial properties of both silicon and carbon, resulting in a material that is mechanically robust, chemically stable, and exhibits tunable electronic characteristics [2]. Unlike crystalline materials, a-SiC lacks long-range order, which provides distinctive advantages in terms of flexibility and the potential for large-area applications [3]. The deposition process [4], particularly the role of precursor gases such as methane, plays a critical role in determining the structural and electronic properties of the resulting films [5]. Understanding the influence of methane flow rate on the electronic properties of a-SiC is essential for optimizing its performance in electronic devices [6].

The deposition of a-SiC typically involves techniques such as plasma-enhanced chemical vapor deposition (PECVD), where methane serves as a carbon source. The methane flow rate during the deposition process can significantly alter the bonding configurations within the material [7]. Specifically, the ratio of sp² (graphite-like) to sp³ (diamond-like) carbon bonds can be modulated by varying the methane flow rate [8], which in turn affects the material's electronic band structure [9]. An increase in methane flow rate generally

leads to a higher concentration of sp^2 bonds [10], which are associated with narrower bandgaps and higher electrical conductivity [11]. Conversely, a lower methane flow rate favors the formation of sp^3 bonds [12], resulting in wider band gaps and reduced conductivity [13]. These variations in bonding and electronic structure underscore the importance of precise control over the deposition parameters to achieve the desired electronic properties in a-SiC films [14].

In addition to the structural and electronic implications, the methane flow rate also impacts the material's defect states and overall film quality. Defect states, which arise from incomplete bonding or impurities, can act as trap sites for charge carriers, thereby influencing the electronic performance of the material [15]. A thorough investigation into the relationship between methane flow rate and the resulting defect states is crucial for optimizing the electronic properties of a-SiC. Advanced characterization techniques, such as spectroscopy ellipsometry, while the surface roughness morphology atomic force microscopy (AFM), are employed to elucidate these correlations. By systematically studying the effects of methane flow rate on the electronic properties of a-SiC, this research aims to provide a comprehensive understanding that will aid in the design and fabrication of high-performance a-SiC-based electronic devices [16]. This knowledge is pivotal for advancing the material's application in cutting-edge technologies, where tailored electronic properties are paramount.

2. RESEARCH METHOD

This investigation used corning glass 7059 substrate, manufactured with indium tin oxide (ITO), to create the p-type layer of a-SiC:H. The two multi-chamber deposition chambers in the PECVD process are designated for the unique purpose of depositing p-type a-SiC:H layers, as seen in Figures 1(a)-1(c). Under these circumstances, the radiation heater temperature (substrate temperature) is the only factor that affects the filament temperature [17]. The source gas is silane gas (SiH_4) that has been concentrated in hydrogen (H_2) to a 10% level. Transparent and able to raise the concentration of charge carriers, methane (CH_4) is added as a p-type layer optimization. Diborane (B_2H_6) gas is used as a dopant gas at a concentration of 10% in H_2 [18]. Table 1 illustrates the growth metrics that were employed.

Table 1. Materials for the a-SiC:H p-type layer to be deposited

Deposition parameters	P-type layer of amorphous silicon carbon (a-SiC:H)	
	P-1	P-2
Flow rate SiH_4	20 sccm	20 sccm
Flow rate B_2H_6	2 sccm	2 sccm
Flow rate H_2	20 sccm	20 sccm
Flow rate CH_4	10 sccm	20 sccm
Power RF	5 Watt	5 Watt
Temperature	210 °C	210 °C
Pressure	4800 mTorr	4800 mTorr
Time	10 minutes	10 minutes

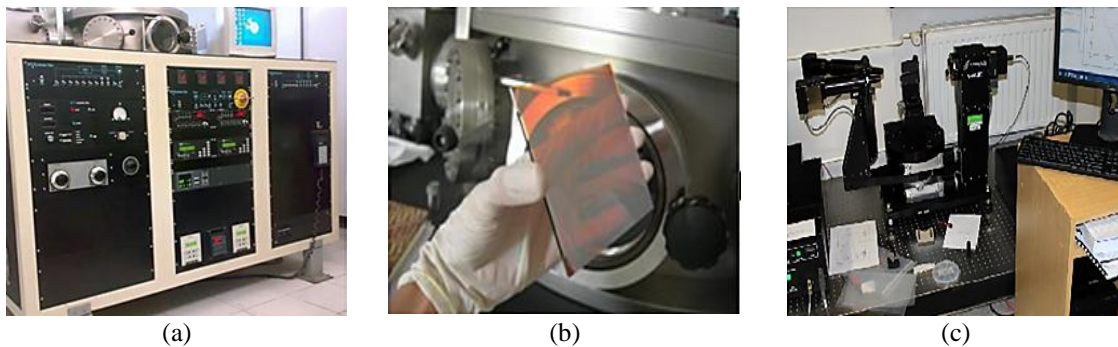


Figure 1. Schematic of p-type a-SiC:H coating sample preparation: (a) PECVD system with a multi-chamber, (b) samples panel p-type layer a-SiC:H (10 x 10) cm² integrated with a conductive film, and (c) spectroscopy ellipsometry (V-VASE, J. A. Woollam Co.)

With spectroscopy ellipsometry (V-VASE, J. A. Woollam Co.) with a rotating analyzer and compensator in Singapore Synchrotron Light Source (SSLS), a photon energy range between 0.6 and 6.5 eV

was measured. The parameters ψ and Δ , which represent the ratio of the amplitude and the phase difference between the reflected light polarized p and s, respectively, were collected on a 70° angle of incidence. With the parameters determined by the surface roughness of the measurement results from P-1 and P-2 atomic force microscopy (AFM), the program employed Woollam Complete Ease to further analyze the fitting of the measurement data. The thickness, roughness, bandgap, and optical constants of the p-type layer of a-SiC were all determined by evaluating each parameter of the dielectric function using a combination of Tauc-Lorentz models (TL)/Tauc-Lorentz+G [19].

The spectroscopic ellipsometry observations on the p-type layer of a-SiC:H are analyzed using the following equation [20]:

- Complex dielectric functions $\varepsilon(\omega) = \varepsilon_1(\omega) + i\varepsilon_2(\omega)$ (ω = the angular frequency of the incident photon).
- Refractive index $n(\omega) = \sqrt{\frac{1}{2}[\sqrt{\varepsilon_1^2(\omega) + \varepsilon_2^2(\omega)} + \varepsilon_1(\omega)]}$
- Extinction coefficient $\kappa(\omega) = \sqrt{\frac{1}{2}[\sqrt{\varepsilon_1^2(\omega) + \varepsilon_2^2(\omega)} - \varepsilon_1(\omega)]}$
- Loss function $-Im[\varepsilon^{-1}(\omega)] = \frac{\varepsilon_2(\omega)}{[\varepsilon_1^2(\omega) + \varepsilon_2^2(\omega)]}$
- The reflectivity of normal incidence $R(\omega) = \frac{[n(\omega)-1]^2 + \kappa^2(\omega)}{[n(\omega)+1]^2 + \kappa^2(\omega)}$

3. RESULTS AND DISCUSSIONS

The results of data fitting are displayed in Figures 2(a) and 2(b), together with the measurements of $\langle\psi\rangle$ and $\langle\Delta\rangle$ for the spectroscopic ellipsometry for samples P-1 and P-2. derived from the sample surface roughness of P-1 and P-2 as shown in Figures 3(a) and 3(b) in order to facilitate the optical and electronic analysis of each sample. The surface morphology of P-1 and P-2 on a $2 \times 2 \mu\text{m}^2$ film area was displayed. It can be observed that there is a high degree of homogeneity between the P-1 and P-2 samples. In samples P-1, the grain size was found to be modest, while samples P-2 showed a larger grain size. This results from modifications to the nucleation process and sample growth brought about by the addition of the methane flow rate [21]. Samples P-1 and P-2 showed that the samples' root-mean-square (RMS) surface roughness values, as determined by AFM measurements, were 8.95 and 6.20 nm.

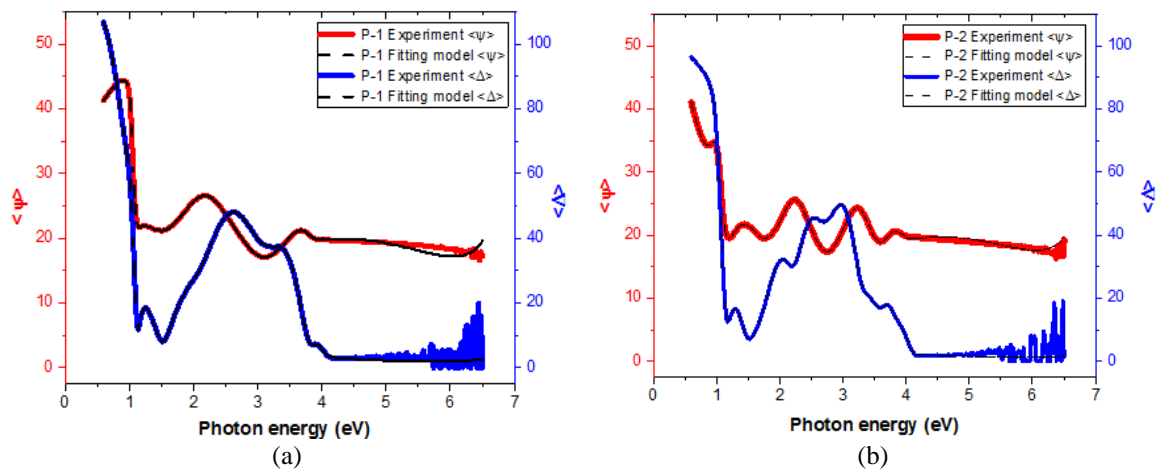


Figure 2. Fittings (point curve) and experimental data (solid curve) from $\langle\psi\rangle$ and $\langle\Delta\rangle$ to (a) P-1 and (b) P-2 obtained using an angle 70° measurement

In the room temperature range of 0.6-6.6 eV, the p-type layer of a-SiC:H was detected. Refractive index, dielectric constant, absorption coefficient, thickness, and roughness of the p-type layer of a-SiC:H are among the metrics and information on the optical properties of materials that were derived from the sample fitting findings for P-1 and P-2. Moreover, each sample's normal incidence reflectivity ($\langle R \rangle$) was determined from the complex dielectric function $\langle \varepsilon_1 \rangle$ and $\langle \varepsilon_2 \rangle$, optical conductivity ($\langle \sigma_1 \rangle$), refractive index ($\langle n \rangle$), and extinction coefficient ($\langle k \rangle$) [22].

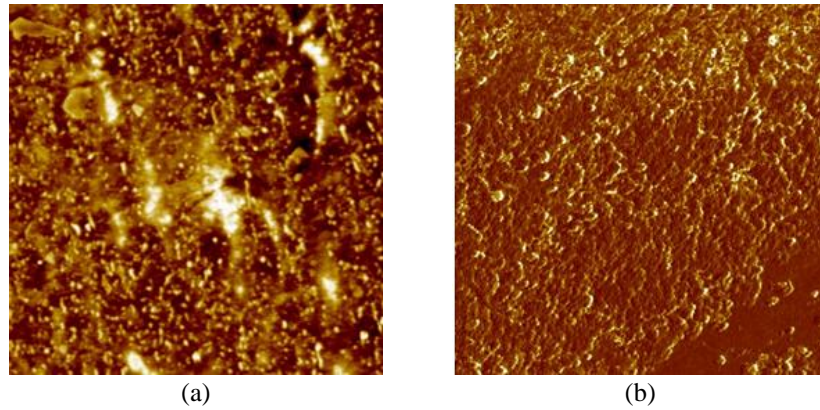


Figure 3. Atomic force microscope measurements that measure (a) surface roughness P-1 and (b) surface roughness P-2

3.1. Complex dielectric function $\langle \epsilon_1 \rangle$ and $\langle \epsilon_2 \rangle$

Throughout the measurement energy range, the material's optical and electrical characteristics are described by the dielectric function $\langle \epsilon \rangle$. The real $\langle \epsilon_1 \rangle$ and imaginary $\langle \epsilon_2 \rangle$ are the two parts of the dielectric function. The amount of light absorption in the material is represented by the imaginary component $\langle \epsilon_2 \rangle$, whereas the real component $\langle \epsilon_1 \rangle$ indicates the polarization of the material caused by the electric dipole, which contributes to the atomic and electric polarization [23]. Samples P-1 and P-2 exhibit values of 2.94 eV and 2.64 eV for E_0 , respectively, as indicated by the real component $\langle \epsilon_1 \rangle$ in Figures 4(a) and 4(b). Sample P-2 is able to absorb more energy than sample P-1 when the E_0 energy changes and this ultimately leads to an improvement in the p-type layer's performance on the solar cell-based p-n a-SiC:H. At that energy, sample P-2 is able to change in energy more than sample P-1 by a large margin (0.3 eV) [24]. Similarly, for the imaginary component $\langle \epsilon_2 \rangle$, the values of E_1 and E_2 , indicative of each sample's excitability, reveal that sample P-2's E_1 and E_2 values change at a lower energy than sample P-1's.

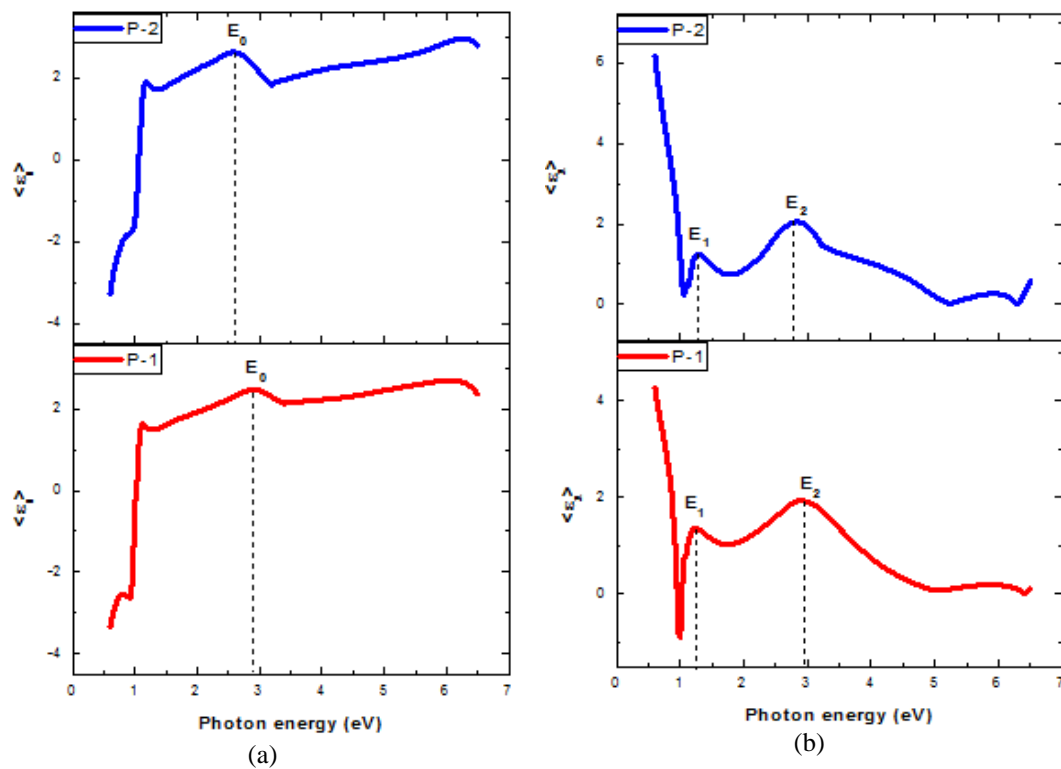


Figure 4. Dielectric function of each layer P-1 and P-2: (a) imaginary part $\langle \epsilon_2 \rangle$ and (b) real part $\langle \epsilon_1 \rangle$

3.2. Refractive index $\langle n \rangle$ and extinction coefficient $\langle k \rangle$

The refractive index of the material, represented by the value of $\langle n \rangle$, and the energy lost due to scattering, represented by the value of $\langle k \rangle$, are the results of spectroscopy ellipsometry measurements [25]. The optical characteristics of sample layers P-1 and P-2 for measurements at the same temperature on the ITO substrate are displayed in Figures 5(a) and 5(b). In comparison to the P-1 sample, the p-type a-SiC:H layer quality in the P-2 sample had a lower n value, indicating that it was of good quality. The maximum absorption rate achieved for sample P-2 is higher than that of sample P-1, despite the fact that both samples are evaluated at the same substrate temperature. This is demonstrated by the very rapid reduction observed at energy <3.0 eV in $\langle n \rangle$ sample P-2 when compared to sample P-1. The temperature of the substrate has a significant impact on how the atoms are deposited and diffuse over it during deposition [26]. The atoms on the substrate's surface will vibrate due to its temperature in this instance, stretching the space between the planes and simplifying the insertion process.

When comparing sample P-2 to sample P-1, the extinction coefficient $\langle k \rangle$ in sample P-2 is found to be 3.0 eV lower, indicating that sample P-2's results are denser. As the flow rate of methane gas increases, the extinction coefficient tends to decrease. The extinction coefficient curves that were obtained have finite energy, meaning that a second layer of p-type a-SiC:H will own its energy price. The value of $\langle k \rangle$, which is in the negative, indicates that a more transparent p-type a-SiC:H layer is created at energies greater than 1.2 eV [27]. This is probably going to lead to atom insertion process saturation, which will produce a less dense layer.

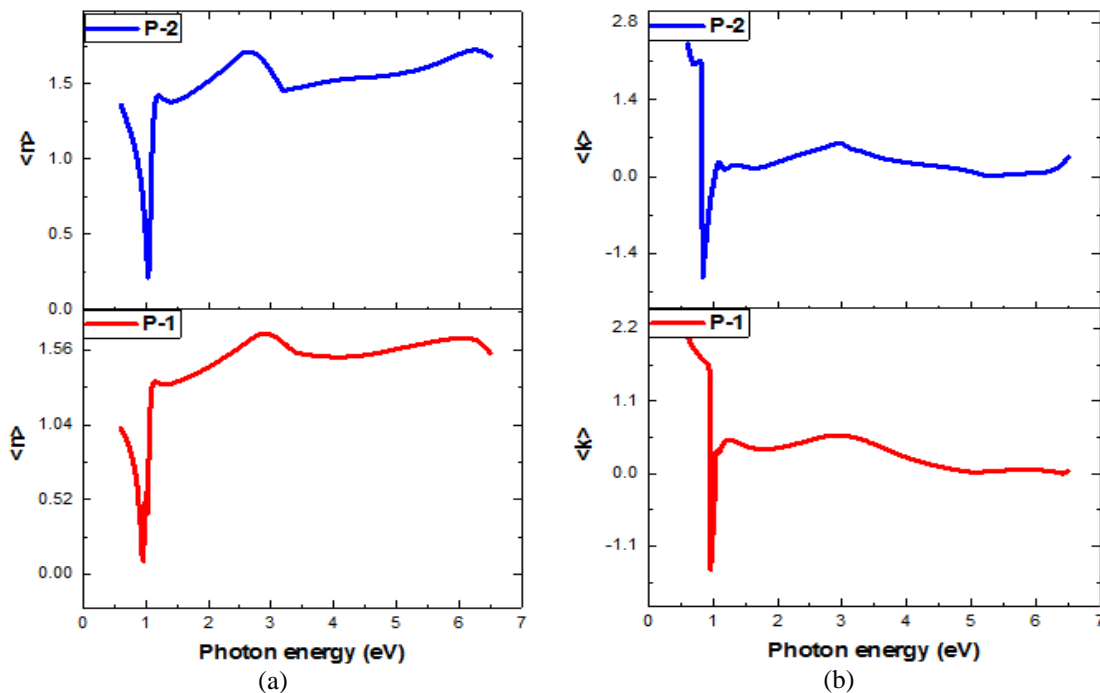


Figure 5. P-1 and P-2 samples' complex refractive indices are (a) $\langle n \rangle$ and (b) $\langle k \rangle$

3.3. Loss-function $\langle -Im [\epsilon^{-1}(\omega)] \rangle$ and normal incident reflectivity $\langle R \rangle$

Loss-function $\langle -Im [\epsilon^{-1}(\omega)] \rangle$ as a function of energy can be derived from the real component $\langle \epsilon_1 \rangle$, and normal incident reflectivity $\langle R \rangle$ can be determined from the imaginary component $\langle \epsilon_2 \rangle$ [28], as seen for the P-1 and P-2 samples in Figure 6. The curve in the figure $\langle -Im [\epsilon^{-1}(\omega)] \rangle$ has shifted, as the flow rate of methane gas increases, to a higher energy at P-2. In this case, a shift to a higher energy and a rise in carbon concentration are related, whereas the shift is caused by the influence of the methane gas flow rate. The curve can be used to determine the a-SiC:H p-type layer's optical gap. Using the definition of energy E_g , that is, the definition of energy right now, we can find the normal incident reflectivity $\langle R \rangle$. Reflectivity of normal incoming light $\langle R \rangle$ valuable >3.0 eV.

Carbon concentration in the p-type layer of a-SiC:H rises with increasing methane flow rate. Using data from hydrogen effusion experiments, NH calculates the amount of hydrogen present in the p-type layer of a-SiC:H. The concentration of hydrogen and the amount of carbon in the p-type layer of a-SiC:H both rise with

an increase in the flow rate of methane gas [29]. The influence of carbon and hydrogen is thus responsible for the effect of the methane gas flow rate on the aforementioned optical quantities [30]. The amount of carbon and hydrogen in the p-type layer will determine the optical gap E_g and the optical magnitude of the refractive index $\langle n \rangle$. The graph illustrates how hydrogen and carbon both raise the optical gap E_g and decrease the refractive index $\langle n \rangle$. The majority of academics believe that rising carbon concentrations are the only factor contributing to the optical gap, however, hydrogen also plays a role [31]. Similarly, despite the fact that methane gas is used as a carbon source throughout the deposition process, the decreased refractive index $\langle n \rangle$ was linked by most researchers to an increase in carbon content.

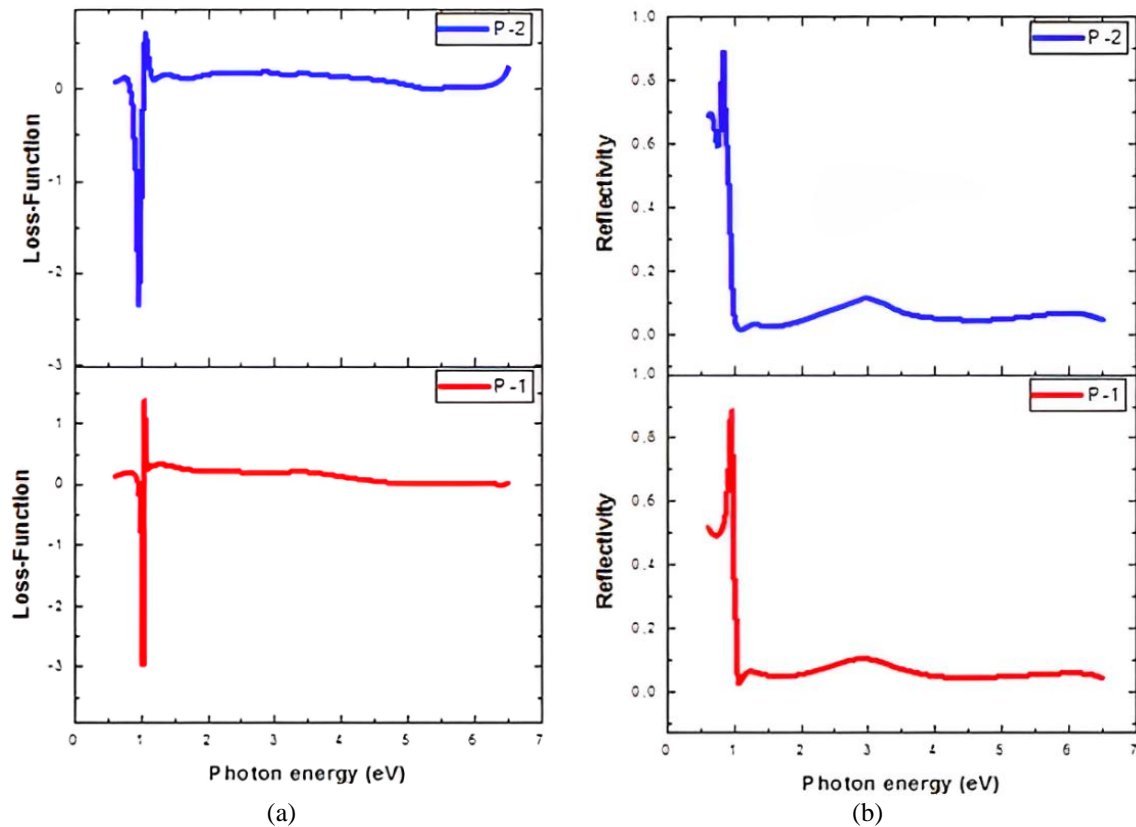


Figure 6. Samples P-1 and P-2: (a) loss-function and (b) reflectivity

4. CONCLUSION

The impact of variations in the methane gas flow rate on the optical properties of the p-type layer a-SiC:H deposition results from the PECVD technique show changes in the form of an increase in the optical gap, a decrease in the value of the dielectric function of the real and imaginary parts, a decrease in the refractive index $\langle n \rangle$ and the E_0 energy in sample P-2 changes in energy to a smaller one than the sample P-1 with a change of 0.3 eV. In the meantime, the addition of amorphous tissue disorder is demonstrated by the impact of increasing carbon composition on the regularity of amorphous tissue. In addition to the amount of carbon in the film, hydrogen is thought to have contributed to the magnitude of the optical layer of the p-type a-SiC:H.




ACKNOWLEDGEMENT

With gratitude, one of the authors (SP) recognizes the financial support provided by the Ministry of Finance of the Republic of Indonesia and Pertamina University. The utilization of experimental facilities at Research Center ITS and SSLS National University of Singapore is also gratefully acknowledged by the authors to LPPM Institut Teknologi Sepuluh Nopember. To measure samples with ellipsometry spectroscopy (V-VASE, J. A. Woollam Co).




REFERENCES

- [1] R. Saleh and N. H. Nickel, "The influence of fermi energy on structural and electrical properties of laser crystallized p-doped amorphous silicon," *Applied Surface Science*, vol. 254, no. 11, pp. 3324–3330, 2008, doi: 10.1016/j.apsusc.2007.11.011.
- [2] A. Nawabjan, F. Iqbal, and A. S. Abdullah, "A front surface optimization study for photovoltaic application," *Telkomnika (Telecommunication Computing Electronics and Control)*, vol. 16, no. 4, pp. 1383–1387, 2018, doi: 10.12928/TELKOMNIKA.v16i4.9059.
- [3] Z. Taliashvili *et al.*, "Optical properties of periodically and aperiodically nanostructured p-n junctions," *Optical and Quantum Electronics*, vol. 55, no. 11, p. 1028, Nov. 2023, doi: 10.1007/s11082-023-05274-x.
- [4] C. Aliani, M. Krichen, and A. Zouari, "Influence of the semiconductor/metal rear contact on the performance of n(a-si:h)/i(a-si:h)/p(c-si) heterojunction solar cells," *Optical and Quantum Electronics*, vol. 50, no. 7, 2018, doi: 10.1007/s11082-018-1555-4.
- [5] H. K. Kaplan, A. Olkun, S. K. Akay, and S. Pat, "Si-based photodiode and material characterization of tio2 thin film," *Optical and Quantum Electronics*, vol. 53, no. 5, 2021, doi: 10.1007/s11082-021-02884-1.
- [6] B. C. Şakar, F. Yıldırım, Z. Orhan, and Aydoğan, "Conduction mechanism and uv/visible photodetection properties of p-si/n-sic heterostructure," *Optical and Quantum Electronics*, vol. 55, no. 4, 2023, doi: 10.1007/s11082-023-04571-9.
- [7] E. Maulana, Rahmadwati, S. N. Sari, and A. Sabarudin, "Optical sensor based on dye-sensitized solar cell with tobacco chlorophyll," *Telkomnika (Telecommunication Computing Electronics and Control)*, vol. 17, no. 4, pp. 1907–1913, 2019, doi: 10.12928/TELKOMNIKA.V17i4.12613.
- [8] J. Fatima Rasheed and V. Suresh Babu, "P+aSixC1-x: h/i-asi:h/n+asi-l-xgex:h graded band gap single junction solar cell with composition graded amorphous silicon carbon alloy as window layer," *Materials Today: Proceedings*, vol. 39, pp. 1910–1915, 2021, doi: 10.1016/j.matpr.2020.08.309.
- [9] N. Watjanatepin and P. Sritanathakorn, "Rectangular module for large scale solar simulator based on high-powered leds array," *Telkomnika (Telecommunication Computing Electronics and Control)*, vol. 20, no. 2, pp. 462–474, 2022, doi: 10.12928/TELKOMNIKA.v20i2.23308.
- [10] R. Gogolin *et al.*, "Analysis of series resistance losses in a-si:h/c-si heterojunction solar cells," *IEEE Journal of Photovoltaics*, vol. 4, no. 5, pp. 1169–1176, 2014, doi: 10.1109/JPHOTOV.2014.2328575.
- [11] R. Saleh and N. H. Nickel, "Boron doped polycrystalline silicon produced by step-by-step xelc excimer laser crystallization," *Materials Research Society Symposium Proceedings*, vol. 910, pp. 635–640, 2007, doi: 10.1557/proc-0910-a23-02.
- [12] M. Valizadeh, I. R. N. Alrubei, H. T. S. Alrikabi, and F. T. Abed, "Enhancing the efficiency of photovoltaic power system by submerging it in the rivers," *Telkomnika (Telecommunication Computing Electronics and Control)*, vol. 20, no. 1, pp. 166–172, 2022, doi: 10.12928/TELKOMNIKA.v20i1.22460.
- [13] Y. Cahyono, U. Maslakah, F. D. Muttaqin, and Darminto, "Reduced energy bandgap of a-si:h films deposited by pecvd at elevating temperatures," *AIP Conference Proceedings*, vol. 1801, 2017, doi: 10.1063/1.4973086.
- [14] R. Saleh and N. H. Nickel, "Silicon-hydrogen bonds in boron and phosphorous doped polycrystalline silicon thin films," *Materials Research Society Symposium Proceedings*, vol. 808, pp. 289–294, 2004, doi: 10.1557/proc-808-a4.4.
- [15] J. Tauc, R. Grigorovici, and A. Vancu, "Optical properties and electronic structure of amorphous germanium," *Physica Status Solidi (B)*, vol. 15, no. 2, pp. 627–637, 1966, doi: 10.1002/pssb.19660150224.
- [16] S. Al-Bediry, R. Taghavi, and A. Bakhshayeshi, "Investigation of structural, electronic, and optical properties of si0.67ge0.33 alloy: a dft approach," *Optical and Quantum Electronics*, vol. 53, no. 6, 2021, doi: 10.1007/s11082-021-02810-5.
- [17] S. Prayogi, Y. Cahyono, I. Iqballudin, M. Stchakovsky, and D. Darminto, "The effect of adding an active layer to the structure of a-si: h solar cells on the efficiency using rf-pecvd," *Journal of Materials Science: Materials in Electronics*, vol. 32, no. 6, pp. 7609–7618, 2021, doi: 10.1007/s10854-021-05477-6.
- [18] S. Prayogi, M. A. Baqiya, Y. Cahyono, and Darminto, "Optical transmission of p-type a-si:h thin film deposited by pecvd on ito-coated glass," *Materials Science Forum*, vol. 966 MSF, pp. 72–76, 2019, doi: 10.4028/www.scientific.net/MSF.966.72.
- [19] M. H. Brodsky, R. S. Title, K. Weiser, and G. D. Pettit, "Structural, optical, and electrical properties of amorphous silicon films," *Physical Review B*, vol. 1, no. 6, pp. 2632–2641, 1970, doi: 10.1103/PhysRevB.1.2632.
- [20] X. J. Y. A. Chaudhuri, K. Rubi, T. C. Asmara, X. Chi, R. Mahendiran, and A. Rusydi, "Quasilocals plasmons in the insulator-metal transition in the mott-type perovskites," *Physical Review B*, vol. 98, no. 16, p. 165303, 2018.
- [21] K. H. Kim, E. V. Johnson, A. G. Kazanskii, M. V. Khenkin, and P. Roca, "Unravelling a simple method for the low temperature synthesis of silicon nanocrystals and monolithic nanocrystalline thin films," *Scientific Reports*, vol. 7, 2017, doi: 10.1038/srep40553.
- [22] P. K. Das *et al.*, "Electronic correlation determining correlated plasmons in sb-doped," *Physical Review B*, vol. 100, no. 11, p. 115109, Sep. 2019, doi: 10.1103/PhysRevB.100.115109.
- [23] G. E. Jellison and F. A. Modine, "Parameterization of the optical functions of amorphous materials in the interband region," *Applied Physics Letters*, vol. 69, no. 3, pp. 371–373, 1996, doi: 10.1063/1.118064.
- [24] J. Song *et al.*, "Degradation of electrical characteristics in low-bandgap polymer solar cells associated with light-induced aging," *Organic Electronics*, vol. 81, 2020, doi: 10.1016/j.orgel.2020.105686.
- [25] J. D. Joannopoulos and M. L. Cohen, "Electronic properties of complex crystalline and amorphous phases of ge and si. i. density of states and band structures," *Physical Review B*, vol. 7, no. 6, pp. 2644–2657, 1973, doi: 10.1103/PhysRevB.7.2644.
- [26] S. Prayogi, Y. Cahyono, and Darminto, "Fabrication of solar cells based on a-si: h layer of intrinsic double (p-i x-i y-n) with pecvd and efficiency analysis," *Journal of Physics: Conference Series*, vol. 1951, no. 1, 2021, doi: 10.1088/1742-6596/1951/1/012015.
- [27] A. Bou *et al.*, "Limited information of impedance spectroscopy about electronic diffusion transport: the case of perovskite solar cells," *APL Materials*, vol. 10, no. 5, 2022, doi: 10.1063/5.0087705.
- [28] X. Yin *et al.*, "Quantum correlated plasmons and their tunability in undoped and doped mott-insulator cuprates," *ACS Photonics*, vol. 6, no. 12, pp. 3281–3289, 2019, doi: 10.1021/acsphotonics.9b01294.
- [29] S. Prayogi, Y. Cahyono, D. Hamdani, and Darminto, "Effect of active layer thickness on the performance of amorphous hydrogenated silicon solar cells," *Engineering and Applied Science Research*, vol. 49, no. 2, pp. 201–208, 2022, doi: 10.14456/easr.2022.22.
- [30] M. M. Moharam *et al.*, "Semiconductors as effective electrodes for dye sensitized solar cell applications," *Topics in Current Chemistry*, vol. 379, no. 3, 2021, doi: 10.1007/s41061-021-00334-w.
- [31] W. Beyer and U. Zastrow, "Dependence of h diffusion in hydrogenated silicon on doping and the fermi level," *Materials Research Society Symposium - Proceedings*, vol. 609, 2000, doi: 10.1557/proc-609-a20.4.




BIOGRAPHIES OF AUTHORS

Soni Prayogi    is currently works as Electrical Engineering, Pertamina University, Indonesia. He does research in materials science, condensed matter physics, and applied science and engineering. He can be contacted at email: soni.prayogi@universitaspertamina.ac.id.



Yoyok Cahyono    currently works as associate profesor at the Department of Physics, Institut Teknologi Sepuluh Nopember (ITS), Surabaya, Indonesia. He conducts research in materials science, semiconductor physics (thin film) with the PECVD technique for solar cell applications. He can be contacted at email: yoyok@physics.its.ac.id.



Darminto    currently works as a professor at the Department of Physics, Institut Teknologi Sepuluh Nopember (ITS), Surabaya, Indonesia. He does research in materials science, condensed matter physics, magnetic compounds, and nano-/2D-materials. His group's current project is 'Development of carbon-based materials from 'green' sources of carbon and functional materials from natural resources for electronic and magnetic applications. He can be contacted at email: darminto@physics.its.ac.id.